

Liquid Metal Oxide-assisted Integration of High-k Dielectrics and Metal Contacts for Two-Dimensional Electronics

*Dasari Venkatakrishnarao¹, Abhishek Mishra¹, Yaoju Tarn¹, Michel Bosman^{1,2}, Rainer Lee¹, Sarthak Das¹, Subhrajit Mukherjee¹, Teymour Talha-Dean^{1,3}, Yiyu Zhang¹, Siew Lang Teo¹, Jian Wei Chai¹, Fabio Bussolotti¹, Kuan Eng Johnson Goh^{*1,4,5}, Chit Siong Lau^{*1,6}*

Keywords: 2D materials, subthreshold swing, field effect transistor, interface engineering, gate leakage, equivalent oxide thickness

¹ Institute of Materials Research and Engineering, Agency for Science, Technology and Research (A*STAR), 2 Fusionopolis Way, Innovis, 138634, Singapore

² Department of Materials Science and Engineering, National University of Singapore, 9 Engineering Drive 1, 117575, Singapore

³ Department of Physics and Astronomy, Queen Mary University of London, London, E14NS, United Kingdom

⁴ Department of Physics, National University of Singapore, 2 Science Drive 3, 117551, Singapore

⁵ Division of Physics and Applied Physics, School of Physical and Mathematical Sciences, Nanyang Technological University, 50 Nanyang Avenue 639798, Singapore

⁶ Science, Mathematics and Technology, Singapore University of Technology and Design, 8 Somapah Road, 487372, Singapore

*Email: aaron_lau@imre.a-star.edu.sg; kejpgoh@yahoo.com

Abstract

Two-dimensional van der Waals semiconductors are promising for future nanoelectronics. However, integrating high-k gate dielectrics for device applications is challenging as the inert van der Waals material surfaces hinder uniform dielectric growth. Here, we report a liquid metal oxide-assisted approach to integrate ultrathin, high-k HfO₂ dielectric on 2D semiconductors with atomically smooth interfaces. Using this approach, we fabricated 2D WS₂ top-gated transistors with subthreshold swings down to 74.5 mV/dec, gate leakage current density below 10⁻⁶ A/cm², and negligible hysteresis. We further demonstrate a one-step van der Waals integration of contacts and dielectrics on graphene. This can offer a scalable approach toward integrating entire prefabricated device stack arrays with 2D materials. Our work provides a scalable solution to address the crucial dielectric engineering challenge for 2D semiconductors, paving the way for high-performance 2D electronics.

The invention of the transistor over a half-century ago was a significant technological breakthrough that accelerated the explosive growth of information technology. Much of modern technological developments can be traced to the role of semiconductor transistors in electronics. Such rapid progress was enabled by Dennard's scaling laws¹ resulting in successful voltage and dimension downscaling of silicon-based complementary metal-oxide-semiconductor (CMOS) technology. The downscaling improved CMOS performance, cost, and energy consumption and paved the way for the growth of CMOS technology projected by the well-known Moore's law.² However, downscaling is approaching its fundamental limits; preserving gate electrostatics when reducing the overall physical device size will require a concurrent reduction in channel thickness.³⁻⁵ However, device performance can degrade when the thickness of silicon is reduced due to increased carrier scattering from surface roughness and dangling bonds.⁶

Therefore, the 'More than Moore' concepts proposed by the International Roadmap for Devices and Systems (IRDS) look beyond silicon at emerging materials.⁷⁻⁹ Two-dimensional (2D) semiconducting transition metal dichalcogenides (TMDs) are an exciting new class of materials for future electronics.^{7,10-16} An attractive advantage of 2D TMDs is their layered van der Waals (vdW) structure, which enables the isolation of monolayers with sub-nm thickness and pristine surfaces lacking

dangling bonds. Thus, unlike silicon, 2D TMD field effect transistors (FETs) can maintain high carrier mobility even at the monolayer limit. Another advantage of 2D TMDs is the wide range of materials with different mechanical, electronic, and optical properties. This is potentially useful for integrating devices with diverse functionalities, including flexible electronics, sensors, and optoelectronics tailored for specific applications, such as artificial intelligence and 'The Internet of Things.'^{5,11,17}

However, dielectric integration remains a challenge in realizing 2D TMD electronics.^{11,18,19} The gate dielectric plays a crucial role in the performance of energy-efficient low-power (LP) devices. Device figures of merit, such as gate leakage current and gate hysteresis, should be minimized for energy efficiency and reliability.^{20,21} The subthreshold swing (SS) quantifies the steepness of the transistor turn-on characteristics and is the gate voltage required to increase the transistor drain current by an order of magnitude. SS should also be minimized; the theoretical thermionic limit is set at 60 mV/dec at room temperature.²² However, in practice, devices are limited by the dielectric and interface quality. Attaining small SS requires a high gate capacitance, which can be achieved by reducing dielectric thickness, but thinner dielectrics can increase gate leakage currents. For example, exfoliated hexagonal boron nitride (hBN) is a commonly used dielectric in laboratories that can be integrated with atomically smooth interfaces. However, the low dielectric constant of hBN is insufficient for thickness scaling while preserving acceptable gate leakage currents.²³ Furthermore, micron-sized exfoliated hBN is intrinsically unscalable. Scalability is also challenging for other vdW dielectrics that have been explored, such as mica,²⁴ CaF₂,^{25,26} MoO₃,²⁷ and SrTiO₃ perovskites.^{28,29}

Alternatively, high-k dielectrics can be deposited, for example, in Intel's 14 nm nodes, where HfO₂ is integrated via atomic layer deposition (ALD).³⁰⁻³² However, ALD is difficult on 2D materials as their pristine surfaces do not promote growth precursor nucleation.³³ ALD-grown dielectrics on 2D materials are typically non-uniform, thin films contain pinholes, and interfaces are rough and defective.^{34,35} The resulting devices have high gate leakage currents, SS values, and gate hysteresis. Surface modification, such as plasma, UV ozone, or metal seeding layers, can promote precursor nucleation.^{32,36-38} However, these techniques damage or alter the 2D material surface and are especially severe in monolayer devices. Seed buffer layers of molecules and polymers can also effectively induce growth nucleation but typically

have low dielectric constants that degrade the gate capacitance and can be thermally unstable.^{39,40}

An emerging strategy is to deposit a dielectric on a sacrificial layer.^{41,42} This sacrificial layer is then etched away to release the dielectric film, which can then be arbitrarily transferred onto a target substrate or over a 2D material of choice. Polymers or graphene can be used as sacrificial layers to integrate dielectrics with 2D TMDs. However, approaches demonstrated so far have restrictions in deposition technique choices and growth conditions due to the limitations of the sacrificial layer. Graphene as a sacrificial layer is incompatible with ALD and is limited to physical deposition techniques like evaporation. Polymers have low thermal stability, limiting growth temperatures and lowering material quality.

Here, we demonstrate the transfer of high-k ALD HfO₂ dielectric using a liquid metal (LM) oxide sacrificial layer. Large-area ultrathin films can be readily transferred without cracks and wrinkles, and atomically smooth interfaces with 2D TMDs can be achieved. Amongst TMDs, MoS₂ is the most studied material due to the availability of high-quality crystals. The less explored WS₂ can potentially offer higher carrier mobility due to its smaller effective mass (~0.3 m₀) and has attracted interest from industry such as IMEC and TSMC.^{43–45} This work explores integrating HfO₂ with 2D WS₂ to form top-gated field effect transistors. The high-quality dielectric integration results in devices with low gate leakage currents < 10⁻⁶ A/cm² well below the IRDS LP limit, negligible gate hysteresis, and record low subthreshold swings of 74.5 mV/dec. We further demonstrate the versatility of our technique with a one-step transfer of both metal contacts and ALD HfO₂ dielectric to form graphene transistors, paving the way toward integrating entire device stack arrays.

Ultrathin LM gallium oxide is the ideal sacrificial layer for transferring dielectrics and metals in many ways. Unlike 2D vdW material surfaces, the hydrophilic gallium oxide surface with dangling bonds is excellent for promoting ALD precursor nucleation.⁴⁶ Furthermore, compared to polymer and graphene-based sacrificial layers, gallium oxide is robust against harsh processes and conditions such as oxygen plasma, UV ozone, and high temperatures above 500 °C (Figure S1).^{47,48} This robustness is crucial for practical versatility and flexibility. A wider range of growth techniques, material choices, and substrate treatment processes can be used to precisely tailor the

properties of the subsequently grown material for specific applications.⁴⁹ The gallium oxide-based sacrificial layer can also benefit the low-temperature back-end of line (BEOL) processes in developing an integrated circuit. It can potentially enable the integration of materials pre-processed at high temperatures, which otherwise cannot be integrated as a BEOL component due to limitations on thermal budget (400 °C). Moreover, this technique can potentially enable integration of various combinations of high-k dielectrics and 2D materials. Such integration can simplify efforts at improving device reliability by finding optimal combinations with respect to defect band alignments, which may otherwise not be possible using conventional direct ALD due to growth limitations.⁵⁰ Next, LM gallium oxides can be printed over large areas (> cm sizes) with excellent uniformity and are ultrathin (~3 nm) and atomically smooth (< 0.3 nm) due to the self-limiting nature of the Cabrera-Mott oxidation mechanism.^{48,51,52} Atomically smooth growth surfaces ensure that ALD-grown materials are uniformly smooth and flat, as ALD is a conformal layer-by-layer growth process. The ultrathin nature of LM gallium oxide as a sacrificial layer reduces excess strain on the grown materials during the thermal cycling of ALD growth that can introduce unwanted cracks and wrinkles.⁴¹ Finally, gallium oxide exhibits excellent etch selectivity with metals and HfO₂, which facilitates its easy delamination for transfer.

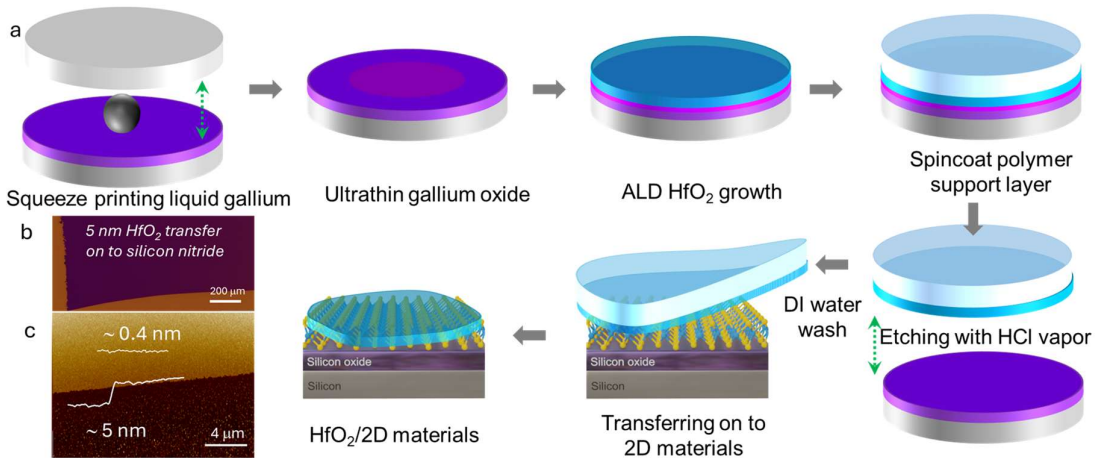


Figure 1 Schematic illustration of liquid metal oxide-assisted HfO₂ transfer. (a) First, ultrathin gallium oxide (~ 3 nm) is printed from liquid gallium metal onto a supporting substrate (SiO₂/Si). The gallium oxide surface is then subjected to O₂ plasma treatment to remove residue and improve its hydrophilicity before atomic layer deposition (ALD) of HfO₂. A polymer support layer is spin-coated for mechanical support before etching away the sacrificial gallium oxide layer with HCl vapor and rinsed with DI water. The HfO₂/polymer stack is then transferred onto a target substrate over 2D materials. (b) Optical microscope image of a large-

area transferred HfO₂ and its (c) atomic force microscopy profile showing a thickness of ~5 nm and a surface roughness down to 0.4 nm.

Figure 1a illustrates this LM-assisted transfer technique for ALD dielectrics. First, we print the sacrificial gallium oxide film from liquid gallium metal onto SiO₂, which acts as a supporting substrate, following the procedure described in our previous work.⁴⁸ Next, a short oxygen plasma treatment is performed to improve the hydrophilicity and cleanliness of the gallium oxide surface in preparation for ALD growth. We grow HfO₂ via ALD at a temperature of 200 °C; its thickness can be precisely controlled through the number of ALD cycles. We then prepare the film for transfer by spin coating a polymer support layer, followed by selective etching of the sacrificial gallium oxide layer using HCl vapor. The polymer/HfO₂ stack is then released and can be transferred onto another target substrate. Large area HfO₂ films up to cm sizes can be achieved (Figure 1b). In principle, even larger films approaching wafer-scale should be possible, which is promising for scalability; we are restricted mainly by equipment limitations, i.e., the size of the LM printing stage.

To first assess the material quality of our HfO₂ films, we perform atomic force microscopy (AFM) and X-ray photoemission spectroscopy (XPS). Our AFM analysis confirms that uniform and smooth HfO₂ films can be transferred with a root-mean-square (RMS) roughness of ~0.4 nm and a thickness down to 5 nm (Figure 1c). The highly stoichiometric HfO₂ films confirmed by XPS (Figure S6) affirm the suitability of LM gallium oxide as a growth substrate for ALD of thin film dielectrics. ALD growth of HfO₂ at 200 °C generally results in amorphous films.⁴⁹ For electronic applications, especially gate dielectrics, amorphous films are preferred over polycrystalline films due to less spatial variations in dielectric properties and suppressed leakage.⁵³

Next, we investigate the interface quality between our transferred HfO₂ films and 2D materials. Figure 2a shows an optical image of a mechanically exfoliated 2D WS₂ flake with mono- and multi-layered regions. Atomic force microscopy analysis conducted on the flake performed before (Figure 2b) and after (Figure 2c) HfO₂ transfer showcases the conformal nature of our dielectric transfer technique. The solid white lines indicate the height profiles measured across the WS₂ edges where we observe no significant changes in step heights after HfO₂ transfer, suggesting that the WS₂/HfO₂ interface remains atomically smooth. This atomic smoothness of the interface is corroborated by cross-sectional scanning transmission electron

microscopy imaging, which directly visualizes the interface morphology for both monolayer (Figure 2d) and multi-layered WS₂ (Figure 2e).

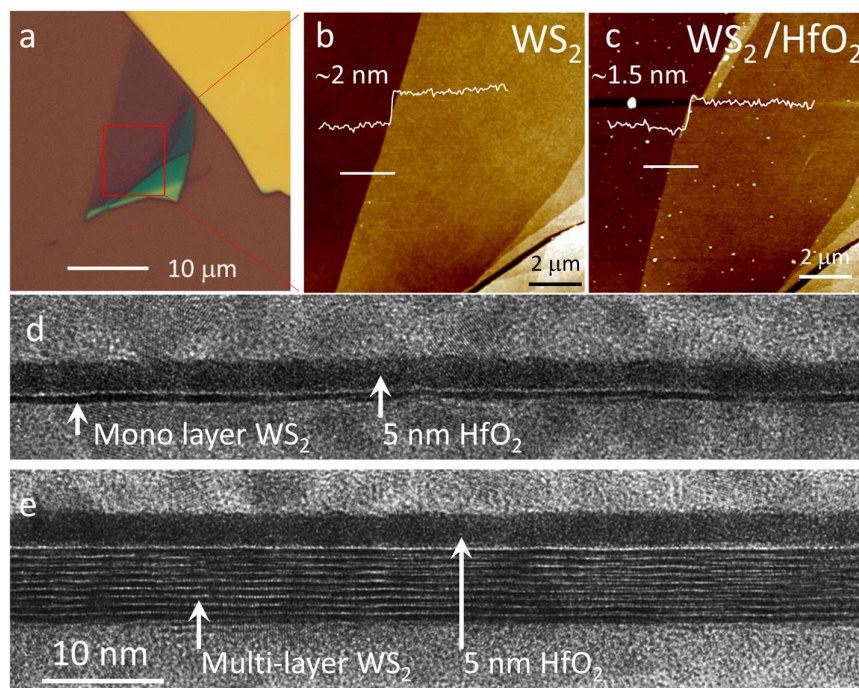


Figure 2 Interface morphology. (a) Optical image of an exfoliated WS₂ flake with monolayer and multilayer regions. Atomic force microscopy image of the WS₂ flake (b) before and (c) after HfO₂ transfer (thickness ~5 nm). The white solid lines indicate where the height profiles are taken. Cross-sectional scanning transmission electron microscopy image (d) mono- and (e) multi-layered WS₂/HfO₂ interface showing an atomically smooth interface.

Such excellent interfacial morphologies should translate to superior electrical characteristics. To assess the electrical properties of transferred HfO₂, we fabricated metal-insulator-metal (MIM) capacitors by transferring HfO₂ onto few-layer graphene/graphite electrodes (Figure 3a). By choosing graphite over conventional metals, we can achieve a sufficiently thin and smooth electrode to minimize mechanical strain in transferred HfO₂, which can be exacerbated when the dielectric film is draped over bulky electrode edges. Such unwanted strain can lead to higher leakage currents or even complete tears and would fail to provide an accurate assessment of our dielectric properties. For comparison, we fabricated MIM capacitors by directly growing ALD HfO₂ on Palladium (Pd) electrodes. With our MIM capacitors, we conducted current-voltage (*I-V*) and capacitance-voltage (*C-V*) measurements (Figure 3b, c). While we observe a slight increase in leakage currents for transferred films compared to as-grown films, overall, the leakage characteristics are excellent (<

10^{-4} A/cm²) and remain well below the IRDS requirement for low-power devices (10^{-2} A/cm²).⁵ Breakdown characteristics are also comparable, at about 6 MV/cm (11 nm) and 7.6 MV/cm (16 nm) for transferred films versus 5.7 MV/cm (11 nm) and 8.7 (16 nm) for direct ALD-grown HfO₂ films. These results affirm the excellent insulating nature of our transferred HfO₂ films.

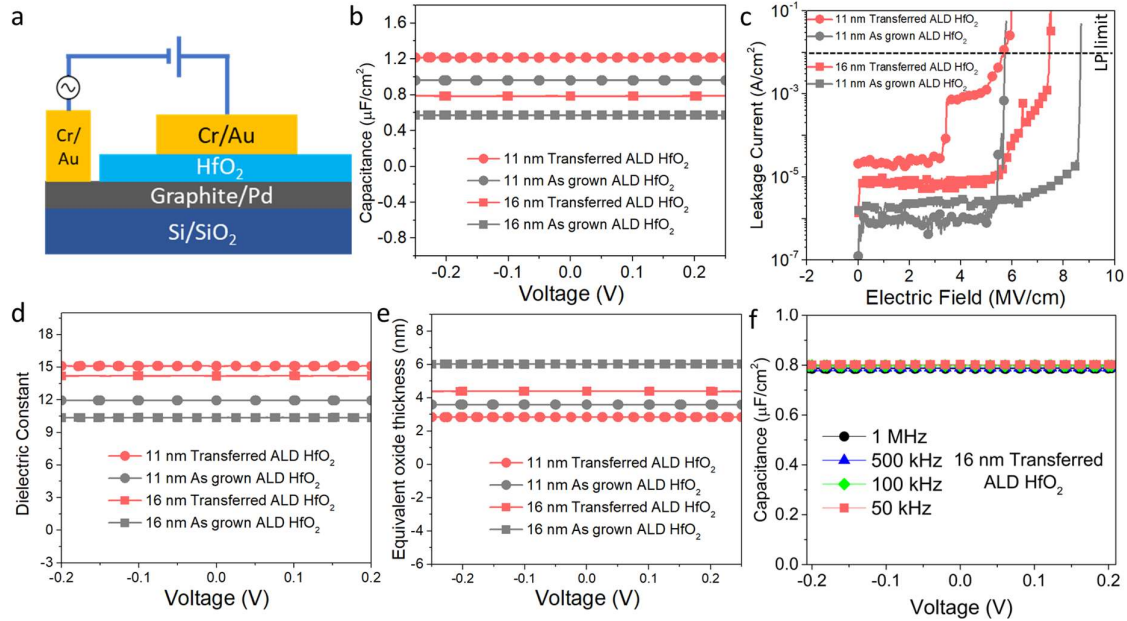


Figure 3 Electrical properties of metal-insulator-metal (MIM) capacitors. (a) Schematic of our MIM devices. For graphite devices, HfO₂ is transferred using the liquid metal-assisted technique. For Pd devices, HfO₂ was directly grown using ALD for comparison. (b) Capacitance-voltage measurements for 11 nm and 16 nm transferred and as-grown HfO₂ films. (c) Breakdown characteristics of 11 and 16 nm transferred and as-grown HfO₂ films. (d) Dielectric constants and (e) equivalent oxide thicknesses are extracted for 11 nm and 16 nm transferred and as-grown HfO₂ films. (f) Capacitance-voltage measurements for the 16 nm transferred HfO₂ device showed only slight variation at different measurement frequencies from 50 kHz to 1 MHz.

From the C-V measurements, we find that the capacitance values for our transferred HfO₂ films (11 nm, 1.2 μ F/cm² and 16 nm, 0.8 μ F/cm²) are slightly higher than their direct ALD-grown counterparts (11 nm, 1.0 μ F/cm² and 16 nm, 0.6 μ F/cm²), further evidence that the integrity and quality of our films are not compromised from the transfer process. High-quality interfaces with low trap densities are confirmed from our C-V measurements, where we find small frequency dispersion across a range of frequencies from 50 kHz to 1 MHz with less than 5% variation in capacitance values.⁵⁴

We next calculate key dielectric parameters such as the dielectric constant $\epsilon_{\text{HfO}_2} = C_{\text{HfO}_2} t_{\text{HfO}_2} / \epsilon_0$ and the equivalent oxide thickness $\text{EOT} = t_{\text{HfO}_2} (\epsilon_{\text{SiO}_2} / \epsilon_{\text{ox}})$, where ϵ_0 , ϵ_{SiO_2} , t_{HfO_2} , and C_{HfO_2} are the vacuum permittivity, silicon oxide dielectric constant, HfO₂ thickness, and HfO₂ capacitance respectively. We find dielectric constants of ~ 15 , consistent with the high-k nature expected of ALD-grown HfO₂ films (Figure 3d).^{46,49} These values translate to small EOTs of 2.8 and 4.4 nm for 11 nm and 16 nm thick HfO₂ films, respectively (Figure 3e). These measurements validate the potential of our technique to integrate high-quality, high-k HfO₂ with 2D materials while preserving excellent interface morphology with low trap density. High-k dielectric integration with atomically smooth surfaces free from interface traps is critical for high-performance 2D electronics. This enables efficient gate coupling to reduce *SS* towards the thermionic limit of 60 mV/dec while maintaining low gate leakage currents and minimal hysteresis for reliable low-power electronics.

To demonstrate this potential for electronic applications, we fabricated 2D WS₂ field effect transistors (FETs). The device architecture is schematically shown in Figure 4a and consists of an *n*-type WS₂ channel with 290 nm SiO₂/Si⁺⁺ as the global back gate and 11 nm HfO₂ as the top gate dielectric. An optical image of the device is shown in Figure 4b. Effective top-gate control is evident from the transfer curves where the drain current *I_D* is measured while sweeping the applied top-gate voltage *V_{TG}* (Figure 4c). The gate leakage current remains negligible, <1 pA/um over the entire gate range (shown in red). Our high-k HfO₂ facilitates efficient gate coupling, and we find a minimum *SS* value of 74.5 mV/dec, approaching the thermionic limit of 60 mV/dec (indicated by the blue slope for comparison). *SS* values remain low as the *I_D* increases with negligible hysteresis between the forward and backward top-gate sweep (Figure 4d). Negligible hysteresis with a width of as small as ~ 3 mV at a back gate voltage *V_{BG}* = 0 V is observed in the transfer curve sweeps due to the low interface trap densities expected for our devices (Figure 4e). More measurements showing negligible hysteresis for different sweep rates are shown in Supporting Information Figure S17. These findings are consistent with measurements of 5 other devices with similarly low *SS* values ranging from 74 - 115 mV/dec, low gate leakage currents from $2\text{-}6 \times 10^{-6}$ A/cm², and negligible hysteresis, as shown in Supporting Information Figure S19-24.

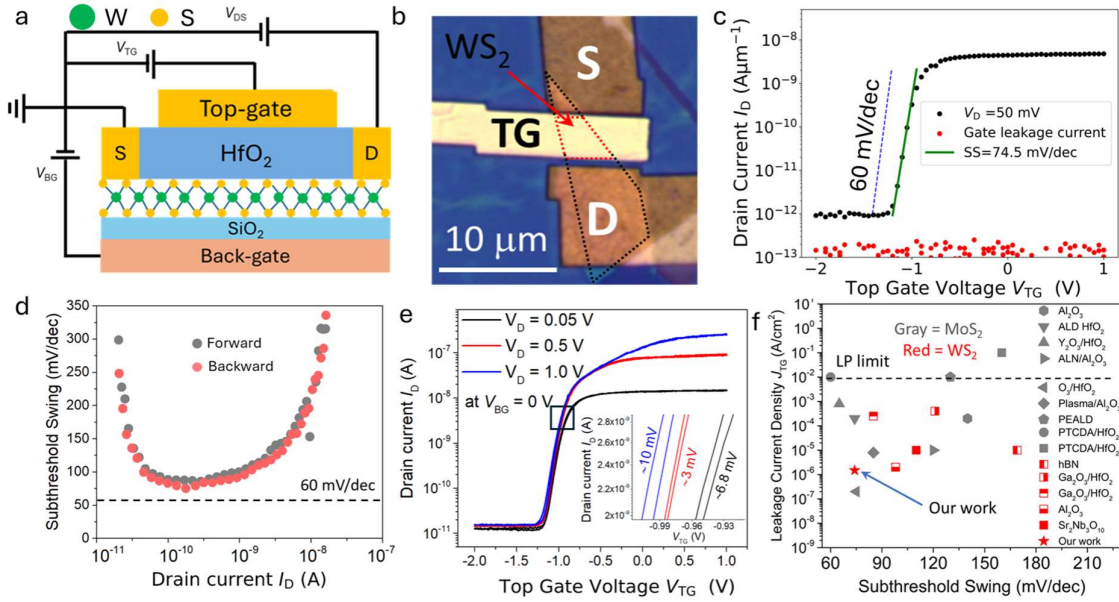


Figure 4 Top-gated WS₂ transistor. (a) Schematic of our transistor architecture with liquid metal-assisted transfer of HfO₂ gate dielectric. (b) Optical image of the device showing the source (S) and drain contacts (D) and the top gate electrode (TG) labeled. (c) Transfer curve of the device, the green line is the fit to extract the subthreshold slope SS of 74.5 mV/dec. (d) SS is determined as a function of the drain current for the forward and backward sweeps. (e) Drain voltage V_D dependent transfer curves at back gate voltage $V_{BG} = 0$ V showing negligible hysteresis at a sweep rate of 0.01 V/s. The inset shows a zoomed-in of the region indicated by the black square highlighting the hysteresis of transfer curves measured at different V_D . (f) Benchmarking of SS and gate leakage current density. Data for the gate leakage currents are measured at $V_D = 1$ V. Due to the lack of data for WS₂ (red), we also include data for MoS₂ (gray), which typically shows better SS values due to lower interface trap densities from higher crystal quality. Our WS₂ transistor shows improved SS and gate leakage current values over other reported WS₂ works and is comparable with MoS₂ devices. More details of the benchmarking data including dielectric thickness is summarized in SI Table 1.

Finally, we critically assess the potential of our dielectric integration technique by benchmarking SS and gate leakage currents with other state-of-the-art approaches for single top-gated 2D transistors. Due to a lack of data available for WS₂ transistors, we also include MoS₂ devices in the benchmarking data. Note that while WS₂ is theoretically superior to MoS₂ for transistor applications due to its smaller effective mass, most experimental realization of 2D MoS₂ transistors outperforms WS₂ due to better material quality. As such, WS₂ transistors typically show higher SS values than MoS₂ transistors of similar architecture due to an increased interface trap density from intrinsic channel defects such as sulfur vacancies.⁵⁵ Nevertheless, our devices still exhibit competitive comparisons with MoS₂, and we demonstrate record-low SS for WS₂ transistors.

While we have focused primarily on LM gallium oxide, HfO_2 , and WS_2 , our approach is not material-exclusive. The transfer technique is generally compatible with other 2D vdW materials. Oxides that can be deposited with ALD or other physical vapor deposition techniques such as sputtering and evaporation should also be possible, e.g., Al_2O_3 and even HfZrO_2 , which raises the intriguing potential for integrating ferroelectric thin films with 2D materials towards novel device architectures like negative capacitance transistors.⁵⁶ Likewise, materials beyond oxides can also be transferred with our approach, such as evaporated metals for contacts. A limitation in our work is that contact metals are first deposited before HfO_2 transfer. This results in a non-flat surface, leading to more significant gaps at the HfO_2 and 2D material interface. Possible solutions are using much thinner electrodes such as graphene or developing selective etching to enable HfO_2 to be transferred before contact fabrication. An even more powerful solution is to develop a single-step process to simultaneously integrate an entire prefabricated device stack that includes metal contacts and oxide dielectrics.⁴² Such devices will have interfaces not compromised by multiple lithography steps during fabrication, which can degrade performance. This makes them attractive for the scalable fabrication of high-quality devices.

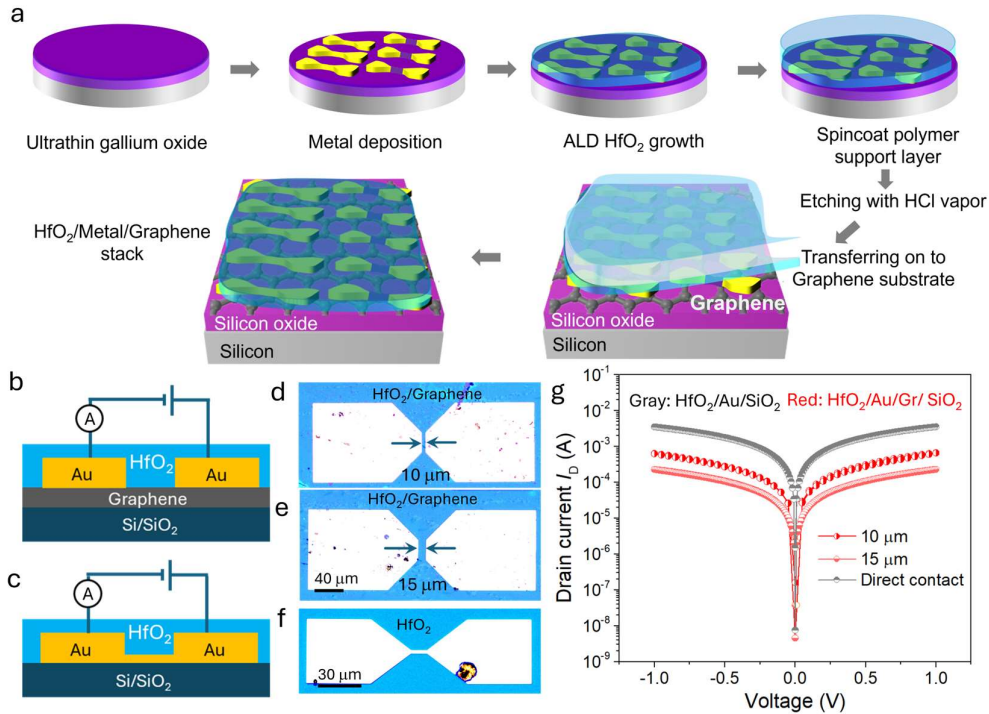


Figure 5 Single-step transfer of dielectric and metal. (a) Schematic illustration of our single-step transfer process of ALD HfO_2 and Au electrodes. Schematic of our devices made from transferring HfO_2 and (b) Au electrodes with varying gap separations onto graphene, or

(c) Au electrodes connected via an Au strip of length 25 μm and width 8 μm . (d-e) Optical images of the transferred Au electrodes with separation gaps of 10 and 15 μm transferred onto graphene. (f) Optical image of the transferred Au electrode connected via an Au strip. (g) Electrical measurements of the devices.

Here, we demonstrate such a proof-of-concept process by transferring simultaneously Au metal and HfO_2 dielectric in a single transfer step. Two types of geometries are shown. The first is Au pads with an area of $\sim 120 \mu\text{m}^2$ connected via an Au strip of length 25 μm and width 8 μm transferred to SiO_2 substrate (Figure 5a,c,f). We also transfer pairs of Au electrodes with varying separations of 10 and 15 μm (Figure 5b,d,e) onto chemical vapor deposition-grown graphene films. The mechanical integrity of the transferred Au is confirmed with electrical measurements of the connected Au electrodes showing a low resistance of $\sim 300 \Omega$ (Figure 5g). Measurements of the devices made from Au electrodes transferred on graphene show 2-10 k Ω resistances, indicating that the transferred Au electrodes can form good electrical contact with CVD graphene. These results demonstrate the potential for vdW integration of entire top-gated device stack arrays using our LM-assisted transfer approach.

Future work should target the optimization and scalability of our transfer process and explore its use for other materials. In principle, much thinner dielectric films should also be possible. Our main challenge working with thinner dielectric films was the poor optical contrast on SiO_2 , which made visual identification difficult (Figure S9). This can be solved through appropriate substrate choices with refractive indices that can maximize optical contrast, as we showed with silicon nitride substrates (Figure 1b, S7c-d).⁵⁷ We also highlight that the LM synthesis approach has already demonstrated several different types of ultrathin oxides experimentally, and theory predicts that as many as fifty more may be possible.⁵² This raises exciting new opportunities to experiment with other LM oxides as sacrificial transfer layers.

To conclude, we reported a LM-assisted integration of high-k ALD dielectric with 2D materials. LM oxides are remarkably suitable as a sacrificial layer to integrate high-quality ALD HfO_2 with 2D materials. WS_2 top-gated transistors fabricated with this approach show excellent performance with low gate leakage currents and record low subthreshold swings promising for low-power applications. We also demonstrate its potential for transferring entire prefabricated device stacks, paving the way toward the

scalable integration of more complex circuits for applications in future nano-electronics.

Methods

Atomic layer deposition: HfO₂ thin films were deposited by atomic layer deposition (ALD) at 200 °C using argon as the purging and carrier gas, with tetrakis-ethylmethylaminohafnium (TEMAHf) and water precursors.

Liquid metal gallium oxide printing: A liquid gallium metal droplet of diameter ~1-3 mm is placed on a top transparent substrate. The top sapphire substrate (width = 1 cm, length = 2 cm) is attached to a micromanipulator to precisely position the liquid metal droplet over the target area where the ultrathin oxide film is intended to be printed. Next, the target substrate is heated up to ~60 °C and brought slowly into contact with the liquid metal droplet. The relative position between the substrates is slowly reduced (~1 μm/s) for the liquid metal droplet to thermally equalize with the heated bottom substrate. As the substrates are brought closer to each other, the liquid metal droplet is 'squeezed' and expands across the substrate surfaces, allowing the oxide skin to spread out and attach to the substrates. Finally, the substrates are brought apart at a rate of ~10 μm/s, leaving behind the ultrathin oxide skin with a roughness ~0.4 nm on the target substrate.⁴⁸ Next, excess liquid gallium residue can be mechanically cleaned by blue tape. Finally, the same sample is used to grow HfO₂ after a short O₂ plasma treatment.

Liquid metal-assisted transfer of ALD HfO₂: Transfer of smaller HfO₂ films is also possible using a polydimethylsiloxane (PDMS) stamp, which is convenient when fabricating vdW heterostructures based on micron-sized exfoliated flakes using a 2D material transfer station. The PDMS is first prepared by mixing the curing agent and base components in a 1:10 ratio. We then degas the mixture in a vacuum before pouring it onto a SiO₂ substrate to cure at 80 °C for 2.5 hours. This layer of PDMS is stripped and applied to a glass slide. O₂ plasma treatment at 100 W, 20 sccm O₂, and 200 mTorr for 5 s ensures effective adhesion between the glass and PDMS layer. We then performed a square cut on our PMMA/HfO₂/Ga₂O₃ stack cut sample. The PDMS is attached to the PMMA/HfO₂/Ga₂O₃ stack and exposed to 1M HCl vapor in a closed vial at 60 °C for ~12h to selectively etch the gallium oxide. More details on the dependence of the etching process on molarity and duration can be found in the SI

Figure S2-3. Next, the etched stack is then immersed in DI water to release the SiO₂ substrate, followed by thorough water washing and vacuum drying to remove residual moisture. Finally, the HfO₂/PMMA/PDMS stack can be transferred onto target substrates using a 2D material transfer stage. Finally, the PMMA is removed with Microposit Remover 1165 solvent.

Device fabrication: Standard electron beam lithography defined contacts and pads. We utilized Nanofrazor thermal scanning probe lithography to define gate electrodes. 5/30 nm of In/Au was evaporated for contacts, and 5/35 nm of Cr/Au was evaporated for the gate electrodes.

Au pads fabrication: The Au pads depicted in Figure 5a were fabricated using electron beam lithography (EBL). Initially, a gallium oxide layer was printed on a SiO₂ substrate, followed by spin coating of a PMMA resist layer to define the desired pad patterns. Subsequently, Au was evaporated onto the substrate, and lift-off was performed using a 1165 solvent with an IPA rinse.

Electrical measurements: Electrical measurements were performed in an electrical probe station using Keithley 2450 SMUs.

TEM and STEM imaging: TEM specimens were prepared by cutting a thin slice of material across the exfoliated WS₂ crystal layer using a Thermo Fisher Helios 450s dual beam focused ion beam system. Imaging was performed with a Thermo Fisher Titan TEM, operated at 200 kV in bright-field TEM mode using an objective aperture that allows the first order diffracted beams of WS₂ to pass, defocusing the beam ~50 nm to further enhance the contrast.

X-ray photoemission spectroscopy: XPS data was acquired using an Al K α source (photon energy $h\nu=1486.7$ eV) and a beam spot size of about 200 μm with an energy resolution of ≈ 0.3 eV. The photoelectrons were collected at a normal emission angle, and the light was incident at 60° to the surface normal. Binding energies were calibrated against the Au 4f core level energy of a gold reference sample. All XPS data was acquired at 300 K.

Optical Measurements: Room temperature photoluminescence (PL) and Raman spectroscopy were conducted using an Invia Raman Renishaw system. Point spectra were acquired with a 532 nm laser through a $\times 100$ objective lens (numerical aperture,

NA = 0.85) and a 2400 lines/mm grating. To prevent any unintentional degradation from laser-induced heating, the excitation power was maintained below 50 μ W. The sample mapping was performed by scanning a $15 \times 10 \mu\text{m}$ area with the same laser excitation for both the pristine sample and the MoS₂ sample covered with transferred HfO₂.

Acknowledgments

This research was supported by the Agency for Science, Technology, and Research (A*STAR) Grant C230917006, MTC YIRG grant No. M21K3c0124 and MTC IRG grant No. M23M6c0103. We acknowledge the funding support from Agency for Science, Technology and Research (#21709). K.E.J.G. acknowledges support from a Singapore National Research Foundation Grant (CRP21-2018-0094).

References

1. Dennard, R. H. et al. Design of ion-implanted MOSFET's with very small physical dimensions. *IEEE J. Solid-State Circuits* **9**, 256–268 (1974).
2. Moore, G. E. Progress in digital integrated electronics [Technical literature, Copyright 1975 IEEE. Reprinted, with permission. Technical Digest. International Electron Devices Meeting, IEEE, 1975, pp. 11-13.]. *IEEE Solid-State Circuits Soc. News*. **11**, 36–37 (2006).
3. Theis, T. N. & Wong, H.-S. P. The End of Moore's Law: A New Beginning for Information Technology. *Comput. Sci. Eng.* **19**, 41–50 (2017).
4. Cao, W. et al. The future transistors. *Nature* **620**, 501–515 (2023).
5. Das, S. et al. Transistors based on two-dimensional materials for future integrated circuits. *Nat. Electron.* **4**, 786–799 (2021).
6. Uchida, K. et al. Experimental study on carrier transport mechanism in ultrathin-body SOI nand p-MOSFETs with SOI thickness less than 5 nm. in *Digest. International Electron Devices Meeting*, 47–50 (2002).

7. Akinwande, D. et al. Graphene and two-dimensional materials for silicon technology. *Nature* **573**, 507–518 (2019).
8. Jayachandran, D. et al. Three-dimensional integration of two-dimensional field-effect transistors. *Nature* **625**, 276–281 (2024).
9. International Roadmap for Devices and Systems (*IEEE*, 2022)
10. Novoselov et al. 2D materials and van der Waals heterostructures. *Science* **353**, aac9439 (2016).
11. Liu, Y. et al. Promises and prospects of two-dimensional transistors. *Nature* **591**, 43–53 (2021).
12. Manzeli, S. et al. 2D transition metal dichalcogenides. *Nat. Rev. Mater.* **2**, 17033 (2017).
13. Chhowalla, M. et al. Two-dimensional semiconductors for transistors. *Nat. Rev. Mater.* **1**, 16052 (2016).
14. Kang, K. et al. High-Mobility Three-Atom-Thick Semiconducting Films with Wafer-Scale Homogeneity. *Nature* **520**, 656 (2015).
15. Wang, Q. H., et al. Electronics and optoelectronics of two-dimensional transition metal dichalcogenides. *Nat. Nanotechnol.* **7**, 699–712 (2012).
16. Fiori, G. et al. Electronics based on two-dimensional materials. *Nat. Nanotechnol.* **9**, 768–779 (2014).
17. Liu, C. et al. Two-dimensional materials for next-generation computing technologies. *Nat. Nanotechnol.* **15**, 545–557 (2020).
18. Illarionov, Y. Y. et al. Insulators for 2D nanoelectronics: the gap to bridge. *Nat. Commun.* **11**, 3385 (2020).
19. Lau, C. S. et al. Dielectrics for Two-Dimensional Transition-Metal Dichalcogenide Applications. *ACS Nano* **17**, 9870–9905 (2023).
20. Lanza, M., et al. Yield, variability, reliability, and stability of two-dimensional materials based solid-state electronic devices. *Nat. Commun.* **11**, 1–5 (2020).

21. Cheng, Z. et al. How to report and benchmark emerging field-effect transistors. *Nat. Electron.* **5**, 416–423 (2022).
22. Ionescu, A. M. et al. Tunnel field-effect transistors as energy-efficient electronic switches. *Nature* **479**, 329–337 (2011).
23. Knobloch, T. et al. The performance limits of hexagonal boron nitride as an insulator for scaled CMOS devices based on two-dimensional materials. *Nat. Electron.* **4**, 98–108 (2021).
24. Zou, X., et L. Long-term stability of multilayer MoS₂ transistors with mica gate dielectric. *Nanotechnology* **31**, 185202 (2020).
25. Illarionov, Y. Y. et al. Ultrathin calcium fluoride insulators for two-dimensional field-effect transistors. *Nat. Electron.* **2**, 230–235 (2019).
26. Illarionov, Y. Y. et al. Reliability of scalable MoS₂ FETs with 2 nm crystalline CaF₂ insulators. *2D Mater.* **6**, (2019).
27. Wang, J. et al. High-κ van der Waals Oxide MoO₃ as Efficient Gate Dielectric for MoS₂ Field-Effect Transistors. *Materials (Basel)*. **15**, 5859 (2022).
28. Yang, A. J. et al. Van der Waals integration of high-κ perovskite oxides and two-dimensional semiconductors. *Nat. Electron.* **5**, 233–240 (2022).
29. Huang, J.-K. et al. High-κ perovskite membranes as insulators for two-dimensional transistors. *Nature* **605**, 262–267 (2022).
30. Song, T. et al. 13.2 A 14nm FinFET 128Mb 6T SRAM with VMIN-enhancement techniques for low-power applications *IEEE J. Solid-State Circuits* **50**, 158–169 (2015).
31. Azcatl, A. et al. HfO₂ on UV-O₃ exposed transition metal dichalcogenides: Interfacial reactions study. *2D Mater.* **2**, (2015).
32. Jadwiszczak, J. et al. Plasma Treatment of Ultrathin Layered Semiconductors for Electronic Device Applications. *ACS Appl. Electron. Mater.* **3**, 1505–1529 (2021).
33. Kim, H. G. et al. Atomic Layer Deposition on 2D Materials. *Chem. Mater.* **29**, 3809–3826 (2017).

34. Lau, C. S. et al. Gate-Defined Quantum Confinement in CVD 2D WS₂. *Adv. Mater.* **34**, 2103907 (2022).
35. Lau, C. S. et al. Carrier control in 2D transition metal dichalcogenides with Al₂O₃ dielectric. *Sci. Rep.* **9**, 8769 (2019).
36. Wang, J. et al. Integration of High-k Oxide on MoS₂ by Using Ozone Pretreatment for High-Performance MoS₂ Top-Gated Transistor with Thickness-Dependent Carrier Scattering Investigation. *Small* **11**, 5932–5938 (2015).
37. Kim, H. et al. Ultrathin monolithic HfO₂ formed by Hf-seeded atomic layer deposition on MoS₂: Film characteristics and its transistor application. *Thin Solid Films* **673**, 112–118 (2019).
38. McDonnell, S. et al. HfO₂ on MoS₂ by atomic layer deposition: Adsorption mechanisms and thickness scalability. *ACS Nano* **7**, 10354–10361 (2013).
39. Li, W. et al. Uniform and ultrathin high-k gate dielectrics for two-dimensional electronic devices. *Nat. Electron.* **2**, 563–571 (2019).
40. Park, J. H. et al. Atomic Layer Deposition of Al₂O₃ on WSe₂ Functionalized by Titanyl Phthalocyanine. *ACS Nano* **10**, 6888–6896 (2016).
41. Lu, Z. et al. Wafer-scale high-k dielectrics for two-dimensional circuits via van der Waals integration. *Nat. Commun.* **14**, 2340 (2023).
42. Wang, L. et al. A general one-step plug-and-probe approach to top-gated transistors for rapidly probing delicate electronic materials. *Nat. Nanotechnol.* **17**, 1206–1213 (2022).
43. Huyghebaert, C. et al. 2D materials: roadmap to CMOS integration. 2018 *IEEE Int. Electron Devices Meet.* 1, 22.1.1-22.1.4 (2018).
44. Lin, D. et al. Dual gate synthetic WS₂ MOSFETs with 120 μ S/ μ m Gm 2.7 μ F/cm² capacitance and ambipolar channel. in Technical Digest - International Electron Devices Meeting, IEDM vols 2020-Decem 3.6.1-3.6.4 (*Institute of Electrical and Electronics Engineers Inc.*, 2020).
45. Su, S.-K. et al. Layered Semiconducting 2D Materials for Future Transistor Applications. *Small Struct.* **2**, 2000103 (2021).

46. Shahin, D. I. et al. Electrical characterization of ALD HfO₂ high-k dielectrics on (2⁻01) β-Ga₂O₃. *Appl. Phys. Lett.* **112**, 1–6 (2018).
47. Tadjer, M. J. et al. Toward gallium oxide power electronics. *Science* **80**, 378, 724–725 (2022).
48. Zhang, Y. et al. Liquid-Metal-Printed Ultrathin Oxides for Atomically Smooth 2D Material Heterostructures. *ACS Nano* **17**, 7929–7939 (2023).
49. Triyoso, D. et al. Impact of Deposition and Annealing Temperature on Material and Electrical Characteristics of ALD HfO₂. *J. Electrochem. Soc.* **151**, F220 (2004).
50. Knobloch, T. et al. Improving stability in two-dimensional transistors with amorphous gate oxides by Fermi-level tuning. *Nat. Electron.* **5**, 356–366 (2022).
51. Zhao, S., Zhang, J. & Fu, L. Liquid Metals: A Novel Possibility of Fabricating 2D Metal Oxides. *Adv. Mater.* **33**, 2005544 (2021).
52. Zavabeti, A. et al. A liquid metal reaction environment for the room-temperature synthesis of atomically thin metal oxides. *Science* **80**, 358, 332–335 (2017).
53. Iglesias, V. et al. Dielectric breakdown in polycrystalline hafnium oxide gate dielectrics investigated by conductive atomic force microscopy. *J. Vac. Sci. Technol. B* **29**, 01AB02 (2011).
54. John, J. W. et al. Probing charge traps at the 2D semiconductor/dielectric interface. *Nanoscale* **15**, 16818–16835 (2023).
55. Sebastian, A. et al. Benchmarking monolayer MoS₂ and WS₂ field-effect transistors. *Nat. Commun.* **12**, 1–12 (2021).
56. Íñiguez, J., et al. Ferroelectric negative capacitance. *Nat. Rev. Mater.* **4**, 243–256 (2019).
57. Li, H. et al. Rapid and Reliable Thickness Identification of Two-Dimensional Nanosheets Using Optical Microscopy. *ACS Nano* **7**, 10344–10353 (2013).

